Magnetism in a graphene-4*f*-3*d* hybrid system

Felix Huttmann,[1,*] David Klar,[2] Nicolae Atodiresei,[3,†] Carolin Schmitz-Antoniak,[2,4] Alevtina Smekhova,[2,4] Antonio J. Martínez-Galera,[1] Vasile Caciuc,[3] Gustav Bihlmayer,[3] Stefan Blügel,[3] Thomas Michely,[1] and Heiko Wende[2]

[1]*II. Physikalisches Institut, Universität zu Köln, Zülpicher Straße 77, 50937 Köln, Germany*

[2]*Fakultät für Physik and Center for Nanointegration (CENIDE), Universität Duisburg-Essen, Lotharstr. 1, 47048 Duisburg, Germany*

[3]*Peter-Grünberg-Institut (PGI-1) and Institute for Advanced Simulation (IAS), Forschungszentrum Jülich, 52428 Jülich, Germany*

[4]*Peter-Grünberg-Institut (PGI-6), Forschungszentrum Jülich, 52428 Jülich, Germany*

(Received 6 November 2016; published 23 February 2017)

We create an interface of graphene with a metallic and magnetic support that leaves its electronic structure largely intact. This is achieved by exposing epitaxial graphene on ferromagnetic thin films of Co and Ni to vapor of the rare earth metal Eu at elevated temperatures, resulting in the intercalation of an Eu monolayer in between graphene and its substrate. The system is atomically well defined, with the Eu monolayer forming a $(\sqrt{3}\times\sqrt{3})R30^\circ$ superstructure with respect to the graphene lattice. Thereby, we avoid the strong hybridization with the (Ni,Co) substrate 3*d* states that otherwise drastically modify the electronic structure of graphene. This picture is suggested by our x-ray absorption spectroscopy measurements which show that after Eu intercalation the empty 2*p* states of C atoms resemble more the ones measured for graphite in contrast to graphene directly bound to 3*d* ferromagnetic substrates. We use x-ray magnetic circular dichroism at the Co and Ni $L_{2,3}$ and Eu $M_{4,5}$ as an element-specific probe to investigate magnetism in these systems. An antiferromagnetic coupling between Eu and Co/Ni moments is found, which is so strong that a magnetic moment of the Eu layer can be detected at room temperature. Density functional theory calculations confirm the antiferromagnetic coupling and provide an atomic insight into the magnetic coupling mechanism.

DOI: 10.1103/PhysRevB.95.075427

I. INTRODUCTION

The desire to either contact graphene (Gr) with magnetic materials or render graphene itself magnetic is motivated by possible spintronic applications [1], due to graphene's negligible spin-orbit coupling and consequently large spin diffusion length [2], as well as the emergence of spin-based quantum effects [3]. A wealth of approaches have been demonstrated: graphene was transferred onto a ferromagnetic insulator [3,4], a ferromagnetic insulator was grown on top of graphene [5,6], ferromagnetic 3*d* metal substrates were used for graphene growth [7], 3*d* [8–11] or 4*f* [12] metals were intercalated after growth on a nonmagnetic substrate, 3*d* metal adatoms were adsorbed [13], or magnetic moments were generated *via* defects that break the graphene AB sublattice symmetry, such as zigzag edges [14–16], hydrogen adatoms [17], vacancies, or voids [18,19].

Graphene on magnetic metallic substrates, such as the extensively studied case of Ni [7,20–22] (and the very similar case of Co [23,24]), is of particular interest, since such an interface can be envisioned as a building block in a spin injection contact of a spintronic device [25,26], and because it can be epitaxially grown, thus representing a highly scalable approach, especially compared to graphite exfoliation. We would like to point out that spin filtering effects at the interface of a metal with graphene (or other π-conjugated carbon systems) do not necessarily rely on a significant induced moment in carbon as has been demonstrated in Refs. [9] and [27–29].

One drawback of the Gr/Ni (or Gr/Co) system, however, is the strong hybridization of the Ni/Co 3*d* electrons with the π system of graphene, which destroys the graphene band structure in a wide window around the Fermi edge [30]. In contrast, a 4*f* metal atom that does not possess a *d* electron, such as Eu, binds mainly ionically to graphene [31], adsorbs in the center of the carbon ring, and thus largely leaves the graphene band structure intact [12]. On the other hand, the ordering temperature of Eu is far below room temperature [12,32].

In the present work, we demonstrate an approach that combines the advantages and avoids the disadvantages of both, using a hybrid 3*d*–4*f* system: to lift the hybridization with the 3*d* states, we employ an Eu monolayer intercalated in between graphene and its Ni or Co substrate, while the 3*d* metal substrate enhances the ordering temperature of the Eu monolayer. Using a combination of experimental and theoretical methods, we show that this system indeed delivers on many of its promises. First, scanning tunneling microscopy (STM) and low-energy electron diffraction (LEED) reveal that the system forms an atomically well-defined interface. Then, temperature- and field-dependent x-ray magnetic circular dichroism (XMCD) measurements provide element-selective evidence that the Eu monolayer becomes magnetically ordered by its contact with the Ni/Co film, even at room temperature. Our *ab initio* density functional theory (DFT) calculations explain the mechanism of magnetic coupling of the Eu and Ni/Co moments and furthermore predict a substantial spin dependence of the π density of states of graphene. The spin-dependent density of states results in a spin polarization at the Fermi level, which could be strongly enhanced by shifting the chemical potential. However, according to our calculations and consistent with experiment the induced net magnetic moment into graphene is marginal. Finally, x-ray absorption spectroscopy (XAS) at the carbon K-edge confirms that the

*huttmann@ph2.uni-koeln.de
†n.atodiresei@fz-juelich.de

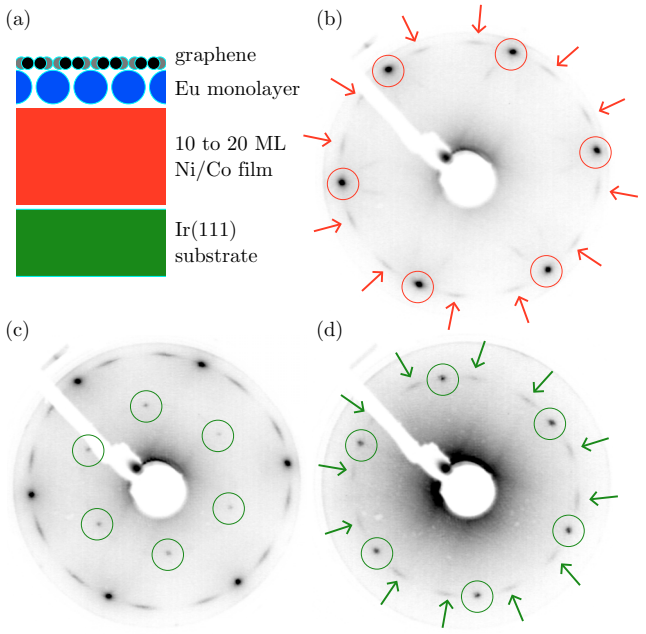

FIG. 1. (a) Schematic cross-sectional sketch [along the substrate's (110) direction] of the investigated system. (b)–(d) Inverted contrast LEED patterns of graphene on Ni thin films. (b) At ≈70 eV electron energy, before intercalation of Eu. (c) Same electron energy as (b), after intercalation of Eu. (d) Same as (b), but at a lower electron energy of ≈36 eV.

substrate hybridization of the π system is lifted and a spectrum close to that of carbon in pristine graphite is recovered.

II. SAMPLE PREPARATION AND METHODS

A schematic cross section of the system that we have studied in this work is depicted in Fig. 1(a). All the samples were prepared and investigated *in situ*. As our substrate we used Ir(111) single crystals cleaned by heating in oxygen, sputtering, and annealing to ≈1500 K. In the next step, Ni and Co films of 10–20 ML thickness were deposited. Such thin films grown on a nonmagnetic substrate are used because they are both easily magnetically saturated by small external fields and already thick enough to be ferromagnetic at room temperature. Graphene on Ni and Co films was then grown by exposing the sample held at 800 K to an ethylene pressure of 2×10^{-6} mbar for 5 min. High-purity Eu [33] was evaporated from a water-cooled Knudsen cell while the sample was at a temperature of 700 K.

Structural characterization was performed with an ultrahigh vacuum (UHV) variable-temperature STM system in Cologne with base pressure $<1\times10^{-10}$ mbar. Images were taken at room temperature. Using the WSxM software [34], plane subtraction and contrast adjustment were applied to the topographs for better visibility. XAS and XMCD measurements were carried out at the PM3 bending magnet beamline of the BESSY II synchrotron facility [Helmholtz-Zentrum Berlin] in the total electron yield mode. In our UHV setup constructed for the measurements at synchrotron radiation facilities the samples were also prepared and measured *in situ*, and the quality of the samples was verified by LEED. XAS and XMCD spectra were acquired under applied fields of 35 mT. To record magnetization loops, the field was changed in small steps. For each field step, the signal at the energy of the maximum of the XMCD is recorded and then normalized to the field-dependent preedge value. Spectra were always taken for both polarizations of incoming light and both external field directions, to avoid nonmagnetic artifacts in the XMCD, yet for brevity, we refer to x-ray helicity parallel (antiparallel) to the external magnetic field only as positive (negative) helicity.

First-principles spin-polarized calculations were carried out using the DFT [35] and the projector augmented plane wave method [36] as implemented in the VASP code [37,38]. A cutoff energy of 500 eV was used for the plane wave expansion of the Kohn-Sham wave functions [39]. The Brillouin zone was sampled with a $(33\times33\times1)$ k-point mesh. To properly account for the nonlocal correlation effects like van der Waals interactions, the structural relaxation was performed using the vdW-DF2 [40] with a revised Becke (B86b) exchange [41–43] functional while for the analysis of the electronic structures we used the PBE exchange-correlation energy functional [44]. To properly account for the orbital dependence of the Coulomb and exchange interactions of the Eu $4f$ states, we employed the GGA + U approach [45] and a Hubbard parameter (U_{eff}) set to 6 eV [46,47]. The supercell contained 15 Å of vacuum in the Z direction and the slab was represented by a graphene layer, an Eu monolayer, and 9 Ni(Co) layers.

III. RESULTS AND DISCUSSION

Figure 1(b) shows a LEED pattern of graphene grown on a Ni thin film. Marked by red circles are the spots of graphene in a (1×1) superstructure with respect to the substrate. Also visible and marked by red arrows are segments of a circle around the central spot, with the same distance from the central spot as the graphene (1×1) spots. These have been previously assigned by Dahal *et al.* [48] to graphene rotated in-plane with respect to the Ni substrate by angles $17\pm7^\circ$.

After exposure of the sample to Eu vapor at elevated temperature, the LEED pattern in Fig. 1(c) has additional spots in the $(\sqrt{3}\times\sqrt{3})R30^\circ$ superstructure position, encircled green. We ascribe this to the formation of an ordered, intercalated monolayer of Eu in between graphene and its metal substrate, as has been previously shown to be the case for graphene on Ir(111) [12]. The LEED pattern seen at a lower electron energy in Fig. 1(d) reveals that segments of an arc of the diameter of the $(\sqrt{3}\times\sqrt{3})R30^\circ$ superstructure spots are also present. It is thus apparent that when the crystallographic directions of graphene and the substrate are rotated against each other, the Eu layer orients by the graphene, rather than by the substrate. We made the same observations also when using a Co instead of a Ni film.

In order to extend our investigation to real space, we have conducted STM measurements on the Ni-based system. Figure 2 shows an STM topograph acquired on a sample where the deposition time was reduced so that only submonolayer amounts of Eu were intercalated. The atomic resolution allows one to identify the (1×1) superstructure of graphene on Ni in the lower part and the $(\sqrt{3}\times\sqrt{3})R30^\circ$ of Eu-intercalated graphene in the upper part of the image. The Eu-intercalation island exhibits a sharp edge which is oriented along the

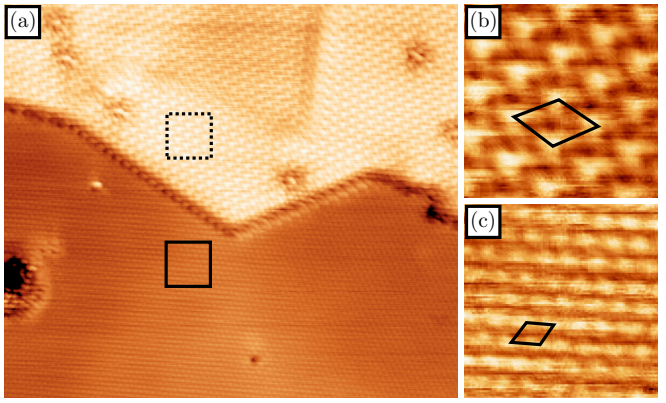

FIG. 2. (a) (20×17) nm^2 STM topograph acquired on partially Eu-intercalated Gr/Ni ($U_B = 190$ mV, $I_t = 150$ nA). (b),(c) (2.1 nm)^2 zoom-in of the area indicated by the dashed/solid square in (a). Unit cells of the $(\sqrt{3}\times\sqrt{3})R30^\circ$ superstructure in (b) and of the (1×1) superstructure of Gr/Ni in (c) indicated by diamonds.

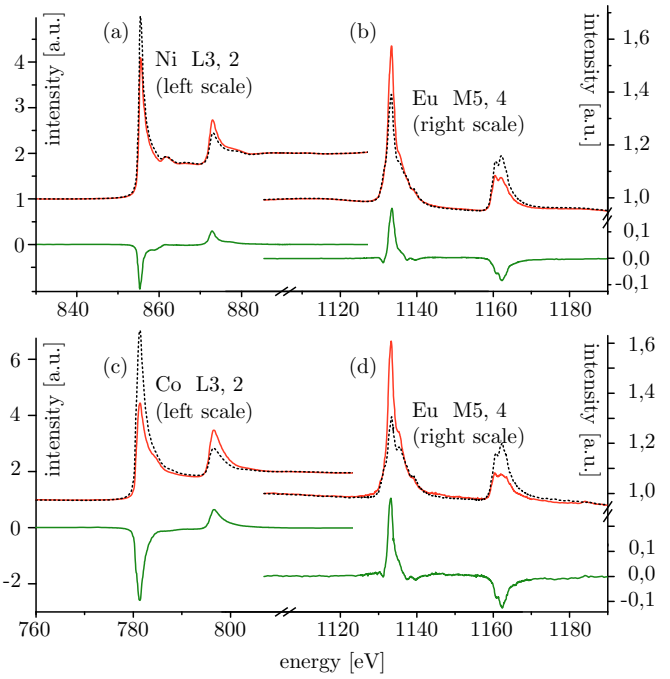

FIG. 3. XAS spectra for different helicities (dashed black and solid red) and resulting XMCD signal (solid green) obtained under grazing incidence at 70 K and in a field of 35 mT for Ni/Co [left side, (a),(c)] and Eu [right side, (b),(d)] in the Gr/Eu/Ni system [upper part, (a),(b)] and Gr/Eu/Co system [lower part, (c),(d)].

dense-packed rows of the Eu layer, rather than the dense-packed rows of Ni or graphene. The small height difference of only about 1 Å between intercalated and nonintercalated regions suggests that the Eu-intercalation island is attached to the lower side of a Ni step edge. We note that, despite the sharp LEED patterns, larger-scale STM images generally showed a high density of obtrusive point defects already prior to Eu intercalation, not untypical for graphene on Ni and previously suggested by Patera *et al.* [49] to result from Ni atoms embedded in the graphene layer. Nevertheless, flat areas could be found where stable imaging is also possible with small tunneling resistances that facilitate higher resolution. Eu intercalation did not cause any measurable increase in the point defect density. Together with the homogenous and well developed $(\sqrt{3}\times\sqrt{3})R30^\circ$ intercalation pattern in intercalated areas and the negligible respective solid solubilities of Eu and Ni [50], we rule out intermixing of Eu and Ni to any significant extent in our samples.

The samples with Eu-intercalated graphene on Ni and Co thin films were investigated by XMCD. In our setup, the magnetic field is always parallel or antiparallel to the beam, while the angle θ between the sample surface normal and the beam can be varied. By comparing the XMCD signals under grazing incidence, shown here, and under normal incidence, with very small XMCD signal, we concluded that our Ni and Co films always exhibited an easy-plane anisotropy. Therefore, all the following measurements have been conducted under 65° grazing incidence.

Figure 3 shows the XAS for different helicities and resulting XMCD of Ni, Co, and Eu measured at the lowest attainable temperature of 70 K. Measurements on the Gr/Eu/Ni system are shown in Figs. 3(a) and 3(b), while measurements on the Gr/Eu/Co system are shown in Figs. 3(c) and 3(d). The obtained XAS and XMCD line shapes of Ni and Co are in agreement with previous observations at their $L_{3,2}$ edges [51,52], confirming that the films are sufficiently thick to be considered bulklike. A comparison of our measurements with Refs. [53,54] clearly indicates that Eu is present in a $4f^7$ configuration, as was previously found also for Eu intercalated under graphene on Ir(111) [12]. More interestingly, however, the XMCD measurements show that the Eu monolayer has a net moment. This moment is antiparallel to the Ni/Co moment as evidenced by the opposite sign of the XMCD signal. Similar coupling has been detected by Sanyal *et al.* [55] for thin layers of Gd on Fe. We have previously shown that an Eu monolayer under graphene on Ir exhibits a net magnetization of comparable size only at a much lower temperature (10 K) and much higher field (≈1 T) [12] indicating a clear magnetic coupling of Eu to the ferromagnetic substrates in the present case. The Eu XMCD signal at 70 K on the Co film is larger than on the Ni film. This points to a stronger coupling of Eu to Co compared to Ni, as we will confirm below. The XMCD line shape for Eu on Co and Eu on Ni is identical, as is the Eu polarization-averaged absorption spectrum (not shown). The polarized Eu absorption spectra on Co and Ni are only slightly different due to incomplete saturation of the Eu moment on the Ni film.

In order to learn more about the relation of the Eu moment to the moment of the underlying 3d metal film, we have measured element-specific magnetic hysteresis loops, which are shown for Eu on Ni in Fig. 4(a). The identical shape of the hysteresis loops of Eu and Ni and their opposite magnetization indicate that the ordering of the moment of the Eu monolayer is induced by an antiferromagnetic coupling with the Ni film.

We performed temperature-dependent measurements of the XMCD signals of Eu and Ni as shown in Fig. 4(b) to investigate the coupling strength. The Ni signal significantly declines only above 400 K, consistent with a bulklike film given the bulk Ni Curie temperature of 627 K. The solid, red line gives

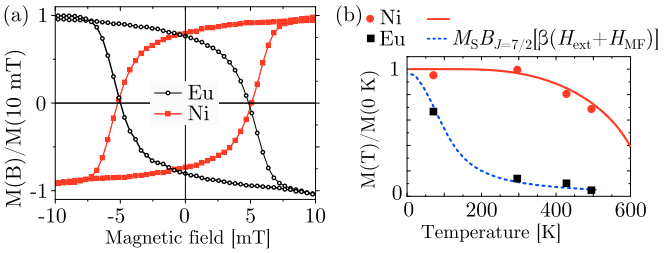

FIG. 4. (a) Hysteresis loop for Eu (red squares) and Ni (black circles) obtained at 70 K. The field was changed stepwise, and for each field the signal at the energy of the maximum of the XMCD is recorded and normalized to the field-dependent pre-edge value. (b) XMCD signals in dependence of temperature for Ni and Eu. Lines are fits to $M(T)$; see text. The XMCD signals are normalized to their expected value at $T = 0$ K as obtained from the respective fits of $M(T)$ for Ni/Eu.

the $M(T)$ curve from mean-field theory, which describes Ni approximately [56].

In contrast, the Eu signal decreases strongly already when going from 70 K to room temperature, yet a nonvanishing XMCD is still detected even at 500 K. A simple mean-field approach is able to describe this: we assume that the Eu monolayer behaves paramagnetically with $J = 7/2$ in an effective external field corresponding to the sum of the actual external field H_{ext} and an exchange field $H_{\text{MF}}(T)$ proportional to the temperature-dependent Ni magnetization, i.e.,

$$M_{Eu} = M_S \cdot B_{J=7/2}[\beta(H_{\text{ext}} + H_{\text{MF}}(T))]. \quad (1)$$

Here, M_S is the saturation magnetization, β is $g\mu_{\text{B}}\mu_0 J/k_B T$, and B is the Brillouin function. We find a good fit to the experimental data as seen in the dashed, blue line in Fig. 4(b), in the process obtaining $H_{\text{MF}}(T = 0\ \text{K}) = (30 \pm 6)\ \text{T}/\mu_0$. For the Co-based system, measurements were only taken at temperatures of 70 and 500 K, and indicated roughly a factor of 2 stronger coupling.

For a better understanding of the magnetic exchange interaction between the Eu atoms and these ferromagnetic substrates, we conducted first-principles calculations. As suggested by our experiments, we used a $(\sqrt{3}\times\sqrt{3})R30^\circ$ surface unit cell. For each system, we found three local energy minima, i.e., the Eu atom adsorbed between 3 Ni (Co) atoms in the (1) fcc or (2) hcp sites and (3) on top of a Ni (Co) atom. In the case of the Ni substrate, the top adsorption site is the most stable (see Fig. 5, left), while the hcp (fcc) adsorption site is higher in energy by 30 meV (75 meV). For the Co substrate the hcp adsorption site is the most stable, followed by the fcc (+20 meV) and top (+141 meV) sites. In the energetically favored adsorption geometry, the difference between the ferromagnetic (FM) and antiferromagnetic (AFM) structures is ≈55 meV for Ni and ≈104 meV for Co, in agreement with the experimental observations that suggest a stronger magnetic exchange coupling between Eu and Co atoms. The preference for antiferromagnetic coupling is not limited to the energetically favored adsorption geometry (see Fig. 5, right): in fact for all optimized Gr/Eu/Ni(111) and Gr/Eu/Co(0001) configurations considered in our study we obtained that Eu is antiferromagnetically coupled to the metal underlayer.

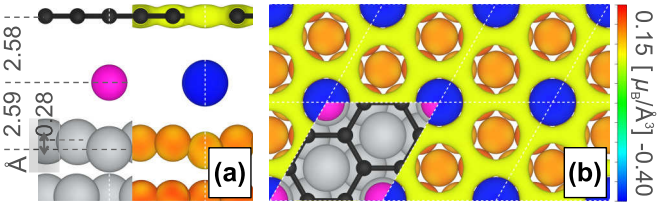

FIG. 5. Ground-state relaxed structure and an isosurface of the total charge density (at $0.2e^-/\text{Å}^3$) colored according to its total magnetization density. for the Gr/Eu/Ni(111) system. (a) Side view along the $[11\bar{2}]$ direction; structure on the left, isosurface plot on the right. (b) Top view along the [111] direction; structure in the rhombus (surface unit cell), isosurface elsewhere. Color code for the structure: C-black, Ni-gray, and Eu-magenta. The crystallographic directions are given with respect to the Ir(111) substrate. Note that the plotted isosurface at the graphene site is ≈0.5 Å away from the carbon atoms. The Ni and C atoms have a positive magnetization (i.e., larger number of electrons in the spin-up channel), while the Eu atoms have a negative magnetization (i.e., larger number of electrons in the spin-down channel).

To compare quantitatively the calculated value for the Eu-Ni magnetic exchange coupling to our experimental results, within a simple model the experimental value can be estimated as $E_{\text{FM-AFM}} = 2\mu_0\mu_{\text{B}} g J H_{\text{MF}}$ to obtain (24 ± 4) meV. The factor of 2 larger exchange coupling constant in theory compared to experiment could be the result of a typical overestimation of the exchange coupling due to self-interaction errors in DFT [57,58].

An isolated Eu atom has the $6s$ orbitals fully occupied, the $5d$ channel is unoccupied, while the f states are half filled. Our theoretical calculations revealed that for the Eu atom intercalated between graphene and the Ni(111) surface, the projection of the total charge density in a sphere around the Eu atom onto the s, p, d, and f atomiclike orbitals leads to the following quantities: 0.10 in s, 0.01 in p, 0.46 in d, and 6.89 in f. The total magnetizations of the atoms are $-7.05\mu_{\text{B}}$ ($5d$: -0.16 and $4f$: -6.89) for Eu, $+0.508\mu_{\text{B}}$ ($3d$) for the Ni below graphene, and $+0.423\mu_{\text{B}}$ ($3d$) for the Ni below Eu atom, while the C atoms acquire only a very small magnetic moment of $\approx 0.004\ \mu_{\text{B}}$. Insofar as the same quantities were computed [i.e., magnetic moment on carbon and graphene-Eu distance in Fig. 5(a)], our results compare well with an earlier theoretical study of this system [59], despite there, a different adsorption position of the Gr/Eu layers relative to the Ni substrate was assumed.

In the following, we would like to discuss the magnetic exchange coupling mechanism. Within an atomic view as proposed by Campbell [60], the antiferromagnetic coupling between Eu $4f$ and Ni $3d$ magnetic moments is mediated by the partially occupied $5d$ orbitals of Eu atoms due to an intra-atomic exchange integral [61,62] of the $4f$ and $5d$ states at the Eu site. It is important to note here that within the Campbell model, the evaluation of the intra-atomic exchange integral [61,62] requires that the atomic $5d$ and $4f$ orbitals are orthogonal to each other.

However, the analysis of the spin-polarized density of states (SP-PDOS) of the C, Eu, and Ni atoms (see Fig. 6) unveils a more subtle scenario that originates from the specific chemical

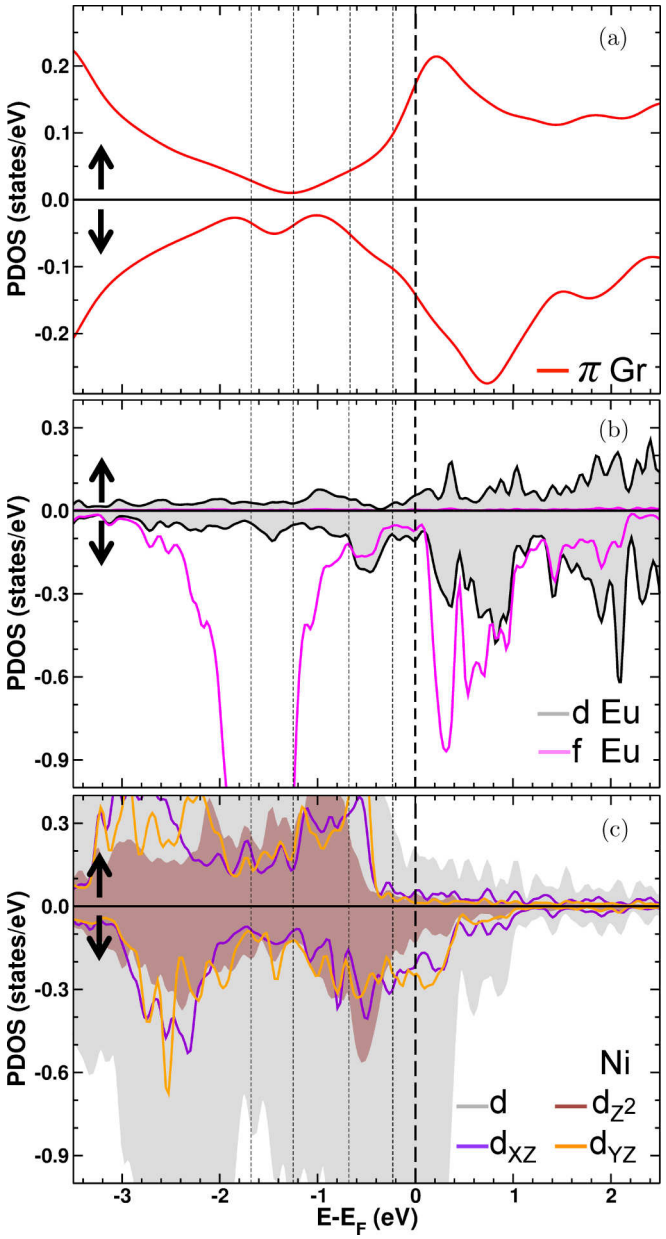

FIG. 6. Spin-polarized local projected density of states (SP-PDOS) of the (a) graphene π orbitals, (b) Eu 4f and 5d states, and (c) surface 3d orbitals of a Ni below Eu. The Gr/Eu/Ni interface hybrid states can be seen in the bonding states indicated by the dotted lines. The black arrows indicate the spin-up and spin-down channels.

environment created by the graphene π electronic cloud and d states of the ferromagnetic substrate. More specifically, an on-site atomic hybridization between the d and f atomic orbitals occurs around the Eu nucleus leading to hybrid atomiclike states with mixed d and f character. For an isolated 4f atom, the f states are very localized in space (close to the nucleus), while the 5d states are much more delocalized over space and their tails extend further away from the atomic core. Hence the on-site atomic hybridization between the d and f states leads to atomiclike df hybrid states at the Eu site with a significant f atomic character close to the ion and extended tails over space that originate from the d-atomic-like orbitals. Due to the long spatial extent, the tails of the Eu atomic hybrid df orbitals can further significantly mix with the π orbitals of graphene and d states of the ferromagnetic substrate. More precisely, the majority spin-down df hybrid states of Eu hybridize with the minority 3d Ni states, which are more reactive due to a larger density of states at the Fermi level. This hybridization leads to an antiferromagnetic coupling between Ni and Eu atoms. Furthermore, due to the spin-dependent hybridization [11,28,63] between π orbitals of graphene and df hybrid states of Eu, graphene develops a spin-dependent electronic structure as seen in Fig. 6(a). These Gr/Eu/Ni interface hybrid states can be clearly seen in the bonding states marked by the dotted lines in Fig. 6. Additionally, the partial occupancy of the d and f channels that also extend over a broad energy range strongly support our suggestion that in the Gr/Eu/Ni(111) system the Eu interacts with the graphene π orbitals and d states of Ni via hybrid atomiclike orbitals that have mixed d and f character. This picture is consistent with similar systems involving the interaction of other 4f metals with π-conjugated organic ligands [64–66]. We note that the on-site Eu df-atomic-like hybrids states are found for all optimized Gr/Eu/Ni(111) configurations. Therefore, the electronic and magnetic structure of Gr/Eu/Ni(111) reported here does not change qualitatively with respect to the Eu adsorption site.

To underpin that the on-site hybridization of the 4f and 5d states is primarily an effect caused by the chemical environment and not just by the higher coordination of the Eu atoms in the Eu layer, we performed a number of additional calculations: for the Eu bulk, an isolated Eu layer, and for an Eu layer on the Ni(111) substrate. For the later two calculations, we used the atomic positions as relaxed in the Gr/Eu/Ni(111) system. We find the following electron occupancy for the Eu 5d channel: Eu layer 0.17, Eu bulk 0.27, Eu/Ni(111) 0.39, and Gr/Eu/Ni(111) 0.46. While the occupation of the Eu 5d channel increases slightly with the atomic coordination number from 0.17 for the Eu layer to 0.27 to Eu bulk, a more substantial increase is caused by the specific chemical environment: from 0.17 for the Eu layer to 0.39 for the Eu layer on Ni(111) and to 0.46 for the Eu layer sandwiched between Ni and graphene. This result is not surprising since by intercalating Eu between graphene and the Ni(111) surface, graphene becomes n doped. As already shown for other systems like Gr/Eu/Ir(111) [43], the n doping of graphene implies the occupation of graphene antibonding π orbitals characterized by a long spatial extent as compared to the bonding ones. Therefore, the overlap of these antibonding π orbitals with the Eu states is expected to be larger as compared to that found between Eu atoms in a bulklike structure.

Despite the small calculated induced magnetic moment of only $0.004\mu_B$ per atom in graphene, the spin-dependent electronic structure in Fig. 6(a) displays a substantial energy-dependent spin polarization. It amounts to about 15% at the Fermi level and reaches a factor of 3 to 4 close to the Dirac point. It would be attractive to exploit the large spin polarization close to the Fermi level, but this would require a considerable shift of the chemical potential by doping.

Considering that the induced magnetic moment on the carbon atom for the Eu-intercalated system is on the order of a factor of 5 smaller than what has been calculated for graphene in direct contact with underlying Co or Ni (for which in

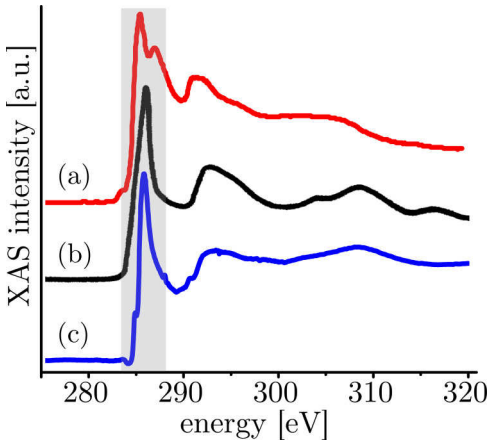

FIG. 7. XAS at the carbon K edge for (a) graphene on Ni (redrawn from Ref. [7]), (b) graphite (redrawn from Ref. [70]), and (c) Eu-intercalated graphene on Ni (own data).

Refs. [7,8] nonvanishing XMCD signals at the C K edge were reported), it is not surprising that our XMCD measurements at the C K edge failed to display an unambiguous dichroic signal. Generally, such measurements are inherently difficult due to the lack of spin-orbit splitting in the carbon 1s initial state of the transition probed by x rays at the K edge, which means that only orbital magnetism can be detected [67–69], and we expect that this orbital magnetic moment is much smaller than the spin moment [67].

Lastly, we discuss the near-edge x-ray absorption fine structure (NEXAFS) at the carbon K edge. Graphite was an early case where features in NEXAFS were directly mapped to transitions into specific valence bands [70]. Figures 7(a)–7(c) show the NEXAFS spectra of Gr/Ni (redrawn from Ref. [7]), of graphite (redrawn from Ref. [70]), and of Gr/Eu/Ni, respectively. Note that our measurements on Gr/Eu/Ni have been performed with circularly polarized x rays at an incidence angle of 65°, while the spectra on graphite and Gr/Ni have been measured with linearly polarized x rays at 60°.

The pronounced feature at ≈286 eV (highlighted with gray background) is a double peak in the case of Gr/Ni, while it is a single peak in the case of graphite. In Refs. [71,72], the double-peak structure has been ascribed to transitions into two interface states that result from the hybridization of graphene π with Ni 3d states. It was furthermore found that upon intercalation of Al, this hybridization is lifted and the single peak as found in freestanding graphene as well as graphite is recovered.

Here, we find that also by intercalation of Eu, the single-peak structure is recovered as seen in Fig. 7(c), demonstrating that graphene can be brought into contact with a magnetic metal without destruction of its electronic structure.

IV. CONCLUSION

In conclusion, we have characterized a system wherein graphene is brought into contact with a Eu monolayer, which is magnetically ordered even at room temperature by its contact with an underlying ferromagnetic film. The Eu monolayer fulfills the purpose of lifting the hybridization of the transition metals 3d and graphene's π orbitals. The slight hybridization between graphene π orbitals and the df hybrid states of Eu results in a spin-dependent electronic structure that could be of interest in spintronic applications.

ACKNOWLEDGMENTS

The authors acknowledge T. Kachel of the BESSY II staff for technical suppport. Financial support was received through the Institutional Strategy of the University of Cologne within the German Excellence Initiative and through the Deutsche Forschungsgemeinschaft Priority Program 1459 "Graphene" within Project No. MI581/20-1, as well as from the Helmholtz-Zentrum Berlin. A.J.M.-G. acknowledges funding by the European Commission. H.W. acknowledges partial financial support by the European Union Seventh Framework Programme, FP7-PEOPLE-2013-IAPP Marie Curie Action: "Industry-Academia Partnerships and Pathways", Project NUMATHIMO and the Deutsche Forschungsgemeinschaft Priority Program 1599 within Project No. WE2623/12-2. The computations were performed under the auspices of the GCS at the high-performance computer JUQUEEN operated by the JSC at the Forschungszentrum Jülich. N.A. and V.C. gratefully acknowledge financial support from the Volkswagen-Stiftung through the "Optically Controlled Spin Logic" project and Deutsche Forschungsgemeinschaft through the Collaborative Research Center SFB 1238 (Project No. C01).

[1] W. Han, R. K. Kawakami, M. Gmitra, and J. Fabian, Nat. Nanotechnol. **9**, 794 (2014).
[2] N. Tombros, C. Jozsa, M. Popinciuc, H. T. Jonkman, and B. J. van Wees, Nature (London) **448**, 571 (2007).
[3] Z. Wang, C. Tang, R. Sachs, Y. Barlas, and J. Shi, Phys. Rev. Lett. **114**, 016603 (2015).
[4] H. X. Yang, A. Hallal, D. Terrade, X. Waintal, S. Roche, and M. Chshiev, Phys. Rev. Lett. **110**, 046603 (2013).
[5] A. G. Swartz, P. M. Odenthal, Y. Hao, R. S. Ruoff, and R. K. Kawakami, ACS Nano **6**, 10063 (2012).
[6] J. Klinkhammer, D. F. Förster, S. Schumacher, H. P. Oepen, T. Michely, and C. Busse, Appl. Phys. Lett. **103**, 131601 (2013).
[7] Y. S. Dedkov and M. Fonin, New J. Phys. **12**, 125004 (2010).
[8] H. Vita, S. Böttcher, P. Leicht, K. Horn, A. B. Shick, and F. Máca, Phys. Rev. B **90**, 165432 (2014).
[9] R. Decker, J. Brede, N. Atodiresei, V. Caciuc, S. Blügel, and R. Wiesendanger, Phys. Rev. B **87**, 041403 (2013).
[10] R. Decker, M. Bazarnik, N. Atodiresei, V. Caciuc, S. Blügel, and R. Wiesendanger, J. Phys.: Condens. Matter **26**, 394004 (2014).
[11] J. Brede, N. Atodiresei, V. Caciuc, M. Bazarnik, A. Al-Zubi, S. Blügel, and R. Wiesendanger, Nat. Nanotechnol. **9**, 1018 (2014).
[12] S. Schumacher, F. Huttmann, M. Petrović, C. Witt, D. F. Förster, C. Vo-Van, J. Coraux, A. J. Martínez-Galera, V. Sessi, I. Vergara, R. Rückamp, M. Grüninger, N. Schleheck, F. Meyer zu Heringdorf, P. Ohresser, M. Kralj, T. O. Wehling, and T. Michely, Phys. Rev. B **90**, 235437 (2014).

[13] T. Eelbo, M. Waśniowska, P. Thakur, M. Gyamfi, B. Sachs, T. O. Wehling, S. Forti, U. Starke, C. Tieg, A. I. Lichtenstein, and R. Wiesendanger, Phys. Rev. Lett. **110**, 136804 (2013).

[14] K. Nakada, M. Fujita, G. Dresselhaus, and M. S. Dresselhaus, Phys. Rev. B **54**, 17954 (1996).

[15] Y.-W. Son, M. L. Cohen, and S. G. Louie, Nature (London) **444**, 347 (2006).

[16] R. Drost, S. Kezilebieke, M. M. Ervasti, S. K. Hämäläinen, F. Schulz, A. Harju, and P. Liljeroth, Sci. Rep. **5**, 16741 (2015).

[17] H. González-Herrero, J. M. Gómez-Rodríguez, P. Mallet, M. Moaied, J. J. Palacios, C. Salgado, M. M. Ugeda, J.-Y. Veuillen, F. Yndurain, and I. Brihuega, Science **352**, 437 (2016).

[18] J. J. Palacios, J. Fernández-Rossier, and L. Brey, Phys. Rev. B **77**, 195428 (2008).

[19] H.-X. Yang, M. Chshiev, D. W. Boukhvalov, X. Waintal, and S. Roche, Phys. Rev. B **84**, 214404 (2011).

[20] F. Mittendorfer, A. Garhofer, J. Redinger, J. Klimeš, J. Harl, and G. Kresse, Phys. Rev. B **84**, 201401 (2011).

[21] F. Bianchini, L. L. Patera, M. Peressi, C. Africh, and G. Comelli, J. Phys. Chem. Lett. **5**, 467 (2014).

[22] A. Barla, V. Bellini, S. Rusponi, P. Ferriani, M. Pivetta, F. Donati, F. Patthey, L. Persichetti, S. K. Mahatha, M. Papagno, C. Piamonteze, S. Fichtner, S. Heinze, P. Gambardella, H. Brune, and C. Carbone, ACS Nano **10**, 1101 (2016).

[23] D. Pacilé, S. Lisi, I. Di Bernardo, M. Papagno, L. Ferrari, M. Pisarra, M. Caputo, S. K. Mahatha, P. M. Sheverdyaeva, P. Moras, P. Lacovig, S. Lizzit, A. Baraldi, M. G. Betti, and C. Carbone, Phys. Rev. B **90**, 195446 (2014).

[24] D. Usachov, A. Fedorov, M. M. Otrokov, A. Chikina, O. Vilkov, A. Petukhov, A. G. Rybkin, Y. M. Koroteev, E. V. Chulkov, V. K. Adamchuk, A. Grüneis, C. Laubschat, and D. V. Vyalikh, Nano Lett. **15**, 2396 (2015).

[25] P. Lazić, G. M. Sipahi, R. K. Kawakami, and I. Žutić, Phys. Rev. B **90**, 085429 (2014).

[26] Q. Wu, L. Shen, Z. Bai, M. Zeng, M. Yang, Z. Huang, and Y. P. Feng, Phys. Rev. Appl. **2**, 044008 (2014).

[27] V. M. Karpan, G. Giovannetti, P. A. Khomyakov, M. Talanana, A. A. Starikov, M. Zwierzycki, J. van den Brink, G. Brocks, and P. J. Kelly, Phys. Rev. Lett. **99**, 176602 (2007).

[28] N. Atodiresei, J. Brede, P. Lazić, V. Caciuc, G. Hoffmann, R. Wiesendanger, and S. Blügel, Phys. Rev. Lett. **105**, 066601 (2010).

[29] J. Brede, N. Atodiresei, S. Kuck, P. Lazić, V. Caciuc, Y. Morikawa, G. Hoffmann, S. Blügel, and R. Wiesendanger, Phys. Rev. Lett. **105**, 047204 (2010).

[30] A. Varykhalov, D. Marchenko, J. Sánchez-Barriga, M. R. Scholz, B. Verberck, B. Trauzettel, T. O. Wehling, C. Carbone, and O. Rader, Phys. Rev. X **2**, 041017 (2012).

[31] D. F. Förster, T. O. Wehling, S. Schumacher, A. Rosch, and T. Michely, New J. Phys. **14**, 023022 (2012).

[32] R. L. Cohen, S. Hüfner, and K. W. West, Phys. Rev. **184**, 263 (1969).

[33] Ames Laboratory (Materials Preparation Center) of the US DOE, Iowa State University, Ames, IA 50011-3020, USA.

[34] I. Horcas, R. Fernández, J. M. Gómez-Rodríguez, J. Colchero, J. Gómez-Herrero, and A. M. Baro, Rev. Sci. Instrum. **78**, 013705 (2007).

[35] P. Hohenberg and W. Kohn, Phys. Rev. **136**, B864 (1964).

[36] P. E. Blöchl, Phys. Rev. B **50**, 17953 (1994).

[37] G. Kresse and J. Hafner, Phys. Rev. B **47**, 558 (1993).

[38] G. Kresse and J. Furthmüller, Phys. Rev. B **54**, 11169 (1996).

[39] W. Kohn and L. J. Sham, Phys. Rev. **140**, A1133 (1965).

[40] K. Lee, E. D. Murray, L. Kong, B. I. Lundqvist, and D. C. Langreth, Phys. Rev. B **82**, 081101 (2010).

[41] A. D. Becke, J. Chem. Phys. **85**, 7184 (1986).

[42] I. Hamada, Phys. Rev. B **89**, 121103 (2014).

[43] F. Huttmann, A. J. Martínez-Galera, V. Caciuc, N. Atodiresei, S. Schumacher, S. Standop, I. Hamada, T. O. Wehling, S. Blügel, and T. Michely, Phys. Rev. Lett. **115**, 236101 (2015).

[44] J. P. Perdew, K. Burke, and M. Ernzerhof, Phys. Rev. Lett. **77**, 3865 (1996).

[45] V. I. Anisimov, F. Aryasetiawan, and A. I. Lichtenstein, J. Phys.: Condens. Matter **9**, 767 (1997).

[46] The results remain practically the same when using a lower (3 eV) or a higher (7 eV) value for U_{eff}.

[47] For the relaxed geometry of the Gr/Eu/Ni(111) system we also performed *ab initio* calculations employing the full-potential linearized augmented plane wave as implemented in the FLEUR code (www.fleur.de). The results we obtained are practically identical with those of our simulations using the VASP code.

[48] A. Dahal, R. Addou, P. Sutter, and M. Batzill, Appl. Phys. Lett. **100**, 241602 (2012).

[49] L. L. Patera, C. Africh, R. S. Weatherup, R. Blume, S. Bhardwaj, C. Castellarin-Cudia, A. Knop-Gericke, R. Schloegl, G. Comelli, S. Hofmann, and C. Cepek, ACS Nano **7**, 7901 (2013).

[50] T. B. Massalski (Editor-in-Chief), H. Okamoto, P. R. Subramanian, and L. Kacprzak, *Binary Alloy Phase Diagrams*, 2nd ed. (ASM International, Materials Park, OH, 1990), Vol. 2.

[51] C. T. Chen, F. Sette, Y. Ma, and S. Modesti, Phys. Rev. B **42**, 7262 (1990).

[52] C. T. Chen, Y. U. Idzerda, H.-J. Lin, N. V. Smith, G. Meigs, E. Chaban, G. H. Ho, E. Pellegrin, and F. Sette, Phys. Rev. Lett. **75**, 152 (1995).

[53] B. T. Thole, G. van der Laan, J. C. Fuggle, G. A. Sawatzky, R. C. Karnatak, and J.-M. Esteva, Phys. Rev. B **32**, 5107 (1985).

[54] D. F. Förster, J. Klinkhammer, C. Busse, S. G. Altendorf, T. Michely, Z. Hu, Y.-Y. Chin, L. H. Tjeng, J. Coraux, and D. Bourgault, Phys. Rev. B **83**, 045424 (2011).

[55] B. Sanyal, C. Antoniak, T. Burkert, B. Krumme, A. Warland, F. Stromberg, C. Praetorius, K. Fauth, H. Wende, and O. Eriksson, Phys. Rev. Lett. **104**, 156402 (2010).

[56] C. Kittel, *Introduction to Solid State Physics*, 8th ed. (John Wiley & Sons, Inc., New York, 2005).

[57] E. Ruiz, S. Alvarez, J. Cano, and V. Polo, J. Chem. Phys. **123**, 164110 (2005).

[58] I. Rudra, Q. Wu, and T. Van Voorhis, J. Chem. Phys. **124**, 024103 (2006).

[59] E. N. Voloshina and Y. S. Dedkov, Z. Naturforsch. A **69**, 297 (2014).

[60] I. A. Campbell, J. Phys. F: Met. Phys. **2**, L47 (1972).

[61] N. H. Duc, in *Intersublattice Exchange Coupling in the Lanthanide-transition Metal Intermetallics*, edited by K. A. Gschneidner and L. Eyring, Handbook on the Physics and Chemistry of Rare Earths Vol. 24 (Elsevier, Amsterdam, 1997), pp. 339–398.

[62] H.-S. Li, Y. P. Li, and J. M. D. Coey, J. Phys.: Condens. Matter **3**, 7277 (1991).

[63] N. Atodiresei, V. Caciuc, P. Lazić, and S. Blügel, Phys. Rev. B **84**, 172402 (2011).
[64] B. Warner, F. El Hallak, N. Atodiresei, P. Seibt, H. Prüser, V. Caciuc, M. Waters, A. J. Fisher, S. Blügel, J. van Slageren, and C. F. Hirjibehedin, Nat. Commun. **7**, 12785 (2016).
[65] A. Candini, D. Klar, S. Marocchi, V. Corradini, R. Biagi, V. D. Renzi, U. del Pennino, F. Troiani, V. Bellini, S. Klyatskaya, M. Ruben, K. Kummer, N. B. Brookes, H. Huang, A. Soncini, H. Wende, and M. Affronte, Sci. Rep. **6**, 21740 (2016).
[66] S. Marocchi, A. Candini, D. Klar, W. Van den Heuvel, H. Huang, F. Troiani, V. Corradini, R. Biagi, V. De Renzi, S. Klyatskaya, K. Kummer, N. B. Brookes, M. Ruben, H. Wende, U. del Pennino, A. Soncini, M. Affronte, and V. Bellini, ACS Nano **10**, 9353 (2016).
[67] C. Sorg, N. Ponpandian, M. Bernien, K. Baberschke, H. Wende, and R. Q. Wu, Phys. Rev. B **73**, 064409 (2006).
[68] H. Wende, Rep. Prog. Phys. **67**, 2105 (2004).
[69] D. Ahlers and G. Schütz, Phys. Rev. B **57**, 3466 (1998).
[70] R. A. Rosenberg, P. J. Love, and V. Rehn, Phys. Rev. B **33**, 4034 (1986).
[71] E. N. Voloshina, A. Generalov, M. Weser, S. Böttcher, K. Horn, and Y. S. Dedkov, New J. Phys. **13**, 113028 (2011).
[72] E. Voloshina, R. Ovcharenko, A. Shulakov, and Y. Dedkov, J. Chem. Phys. **138**, 154706 (2013).